Influence upon cycling of oxygen amount in tin-based compound used as negative electrode in lithium-ion battery

Charlotte Gervillié, Aurélie Boisard, Julien Labbe, Sandrine Berthon-Fabry, Katia Guérin

Influence upon cycling of oxygen amount in tin-based compound used as negative electrode in lithium-ion battery

Charlotte Gervillié[1, 2, 3], Aurélie Boisard[3], Julien Labbé[3], Sandrine Berthon-Fabry[1*], Katia Guérin[2*]

1. *MINES ParisTech, PSL University, Centre for processes, renewable energies and energy systems (PERSEE), CS 10207 rue Claude Daunesse, 06904 Sophia Antipolis Cedex, France*
2. *Université Clermont Auvergne, SIGMA Clermont, CNRS, ICCF, 24, Avenue Blaise Pascal, 63178 Aubière, France*
3. *Safran Tech, SAFRAN, Rue des jeunes Bois, 78117 Châteaufort, France*

*Corresponding authors:
Katia Guérin: katia.araujo_da_silva@uca.fr
Sandrine Berthon-Fabry : sandrine.berthon-fabry@mines-paristech.fr

Abstract

Electrochemical and physicochemical characteristics of three tin-based materials with various oxygen amount used as negative electrode in lithium-ion battery have been evaluated and compared. Nanosizing structuration impact in case of SnO_2 is also discussed. Depending on the oxygen amount in those materials used as electrode, energy and power density of lithium-ion battery can be modulated up to 2000 Wh/kg and 8000 W/kg for a maximum sustainable 3C rate. Fading depends mainly on the oxygen amount and, to a lesser extent, on nanostructuration. SnO appears as the best candidate in this material family concerning irreversible capacities and coulombic efficiency. Post-mortem characterizations after 100 cycles by XRD, SEM and EDX highlight a lower aggregation of tin particles for oxygen-based materials upon cycles and formation of α- crystallographic tin phase which can be supposed as beneficial for coulombic efficiency.

Keywords—Li-ion battery, negative electrode, tin-based materials, post-mortem analysis, galvanostatic measurements

Graphical Abstract

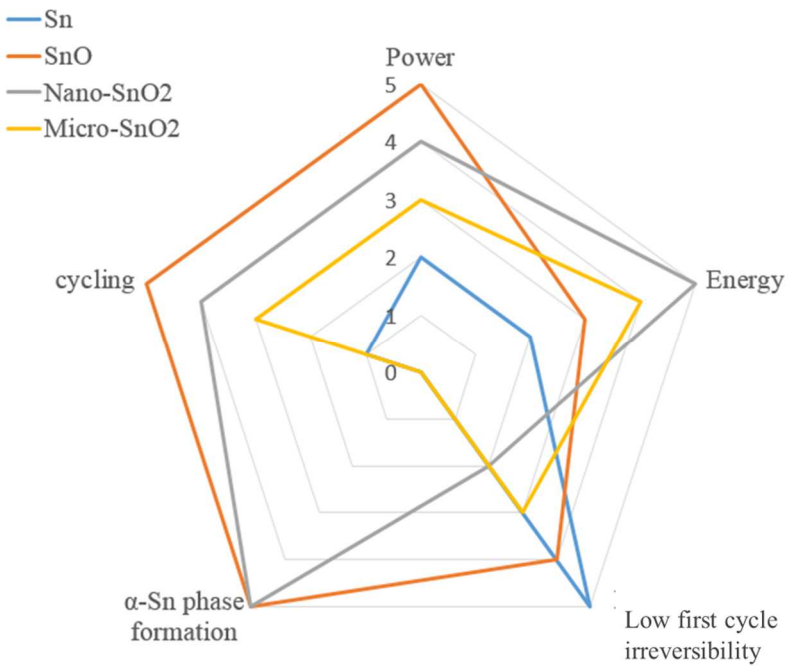

1. Introduction

Rechargeable lithium-ion batteries (LIBs) have overwhelmed the consumer electronics market and thus have become the promising power sources for electric transports as electric vehicles (EVs) and hybrid vehicles (HEVs) [1], [2]. The electric powered idea has also begun to take-off flight applications. If commercial airplane are far to have an electric propulsion, they already integrate battery as backup batteries or for starting the auxiliary power unit (APU) for examples [3]. In another part, many projects of aerial taxi are developed. At this small scale, the electric propulsion make sense [4]. In this way, in 2019, Uber Company in partnership with Bell introduced during the CES (Consumer Electronic Show) in Las Vegas its first taxi/drone. Bell entrusted the French company Safran the task to motorize the aircraft. This prototype called "Nexus" is a vertical takeoff and landing vehicle (VTOL). Safran offers hybrid propulsion (a turbogenerator and a battery provide energy). For the Uber VTOL applications, the battery cell specific energy required is 400 Wh/kg. The electric VTOLs will likely use large battery packs nominally a 140 kWh pack for a 4 person aircraft [5]. However, the battery specifications are relative to the manufacturers [6]. For example, the requirement for the E-Hang 184 (which is also describe as an UAV capable of carrying passengers) is a battery pack of energy density of 14.4 kWh ie 21.6 Wh at cell scale, a battery life of 1000 cycles at 1C and a 3C maximum charge rate [7].

In addition to electric transport applications, the market for lithium-ion continues to grow rapidly due to their use ranging from stationary storage of renewable energy to powering all electronic devices such as phones and laptops [8], [9]. In consequence the development of new promising materials with high energy density is required [10], [11].

Today, negative electrodes for lithium ion battery have a limited specific capacity ($C_{graphite}$=372 mAh/g), leading to a maximum energy density of 14.4 kWh.

Tin-based materials family is one of them because of its high capacity (993 mAh/g). Tin is also a very abundant and non-toxic material with low lithiation/delithiation potential versus Li^+/Li and high electronic conductivity [12]. However, the lithium ion electrochemical process of tin differs from the well-known insertion one and is a major limitation to its industrial application. Indeed, Sn electrode undergoes severe volume expansion (up to 300% for $Li_{22}Sn_5$ [13]) and contraction during cycling. This leads to particle fragmentation. This phenomena is called "electrochemical grinding" and leads to delamination and electronic contact loss [14]. In addition, the coexistence of massive Li-Sn alloy phases within the same particle creates a phase boundary between adjacent phases that have different crystal structures and Li:Sn ratios - and thus different volumes. As a result, the different regions within a particle, break away and become inactive [15], [16].

To solve these problems, SnO_x has been considered as a promising candidate to improve the tin material performances [17]. Its fabrication and design have been widely reported. For the SnO_2 material, two electrochemical reactions take place [13], [18]: First, the partially irreversible conversion of tin oxide into tin particles enclosed into a Li_2O matrix occurs (1). Then, tin particles are able to form different alloys with lithium up to the theoretical limit of $Li_{4.4}Sn$ following the equation (2). This last reversible mechanism will drive the electrochemical activity.

$$SnO_2 + 4Li^+ + 4e^- \rightarrow Sn + 2Li_2O \quad (1)$$

$$Sn + xLi^+ + xe^- \leftrightarrow Li_xSn \ (0 \leq x \leq 4.4) \quad (2)$$

Li_2O formation appears as very slowly reversible in special conditions [19]. Hu et al. showed that the Li_2O formation can be highly reversible with controlled nanostructure of SnO_2 using in situ SERS (surface-enhanced Raman spectroscopy) study [20]. However, in most of the case the electrochemical performances come from the alloying process. The conversion mechanism for tin oxide material has been issued as beneficial to the stability of the electrode but a high irreversible capacity is lost during the first cycle. The oxide matrix acts as a buffer to protect the particles and limits their aggregation [21]. Retoux et al. showed using high resolution microscopy coupled with electronic diffraction that the decomposition of SnO_2 into 10 to 50 nm tin grains surrounded by a 5 to 10 nm amorphous matrix made of Sn and O. They also proved that the size of tin particles increased upon cycling due to aggregation [22]. SnO (II) has been much less reported [13]. However, one advantage using SnO rather than SnO_2 is that the loss of Li ions is reduced [23], the conversion step becoming:

$$SnO + 2Li^+ + 2e^- \rightarrow Sn + Li_2O \quad (3)$$

So, tin-based materials including oxides, sulfides, intermetallic, alloys and some other compounds have attracted many attention and been intensively studied in the past decades [12]. However, only few articles compare their performances in the same electrochemical conditions, and an important lack of data on tin (II) oxide [12], [24], [25] exists.

In this publication, we have done a systematic study of different tin-based materials used as electrode in lithium-ion battery and tested in the same electrochemical conditions. Thanks to the different means of characterization (X-ray diffraction XRD, Scanning electron spectroscopy SEM coupled with EDX), we aim at comparing and then explaining, the different performance, in half cell, of tin-based materials during the first cycles. Post-mortem characterizations have been done in order to investigate the failure mode upon 100 cycles of these materials. A major attention is paid to the influence of oxygen content and of nanostructuration.

2. Materials and methods

Sn (Tin nanopowder from Sigma Aldrich), SnO (Tin (II) oxide powder from Sigma Aldrich), micro-SnO_2 (Tin (IV) Oxide from Sigma Aldrich) and nano-SnO_2 (Tin (IV) oxide nanopowder from Sigma Aldrich) have been characterized by scanning electron microscopy (SEM) ZEISS SUPRA operating at 3 kV. X-ray diffraction (XRD) patterns were collected using a System X'pert pro diffractometer with a Cu Kα radiation source between 20 and 90°. The diffractogram patterns have been refined using Rietveld method in FullProf program.

The electrochemical properties of tin-based materials were studied at room temperature in CR2032 coin cells with lithium metal as negative and reference electrode. The working electrode preparation consisted of 70% of active material, 20% of conductive agent (Y50 from Imerys Graphite & Carbon) and 10% of binder (PVDF HSV9000. The electrode

was dried at 105°C for 2 hours. A Whatman glass fiber was saturated with 1M $LiPF_6$ EC:PC:DMC (1:1:3) mixture electrolyte, and insulated from the electrode with two celgard separators. The coin cell was assembled in an argon-filled glove box. Galvanostatic measurements were carried out between 0.05 and 3V (vs Li/Li^+) at 40 mA/g for long cycling (C/25 considering the theoretical capacity of tin) or at current densities up to 2560 mA/g for 1 cycle on a Biologic battery testing system. The electrochemical results were calculated based on the active mass, related exclusively to the tin-based material one and have been reproduced almost 3 times.

For post-mortem analysis, the cells have been opened at the end of oxidation process after 100 cycles at 40 mA/g in galvanostatic regime, washed with PC solvent and dried softly in glove box. Then, the electrodes have been characterized by XRD and SEM coupled with EDX.

3. Results and Discussion

3.1. Material characterizations

XRD patterns of some different commercially available tin-based materials are presented in Fig. 1. The patterns have been refined using Le Bail refinement. Sn can be indexed to tetragonal β-Sn structure with a $I4_1/amd$ space group (a_{th} = 5.8317 Å, c_{th} = 3.1813 Å). Some SnO impurities are observed with a space group P4/nmm (a_{th} = 5.832 Å, c_{th} = 3.181 Å) [26], [27]. Indeed, tin can be partially oxidized under air [28]. SnO powder pattern can be indexed to the SnO structure, whereas nano and micro-SnO_2 to rutile SnO_2 structure P42/mnm (a_{th} = 4.738 Å, c_{th} = 3.187 Å). All the materials have a good crystallinity and a good phase purity except for Sn.

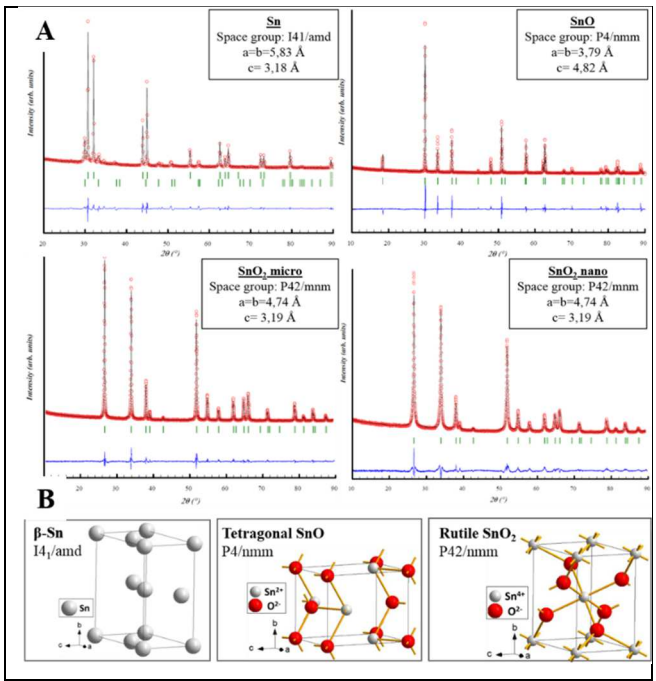

Fig. 1. (A) XRD patterns and Le Bail refinement of Sn, SnO, nano-SnO_2 and micro-SnO_2. (B) Structure of the different tin-based materials.

Fig. 2 shows SEM images of the different materials. The Sn powder is composed of spherical particles with an important diameter distribution between 50 and 500 nm. SnO powder is black which corresponds to its stable phase. Observed by SEM, SnO is composed mostly of micrometric particles. At highest magnifications, a tabular crystal structure can be observed with a face size of about 5 µm. SnO is metastable in ambient conditions but can be oxidized in air following the equation (4). The oxide can also undergo the reaction described in equation (5) even in the absence of oxygen [29], [30].

$$2SnO(s) + O_{2(g)} \rightarrow 2SnO_{2(s)} \quad (4)$$

$$2SnO_{(s)} \rightarrow SnO_{2(s)} + Sn_{(l)} \quad (5)$$

Observations of smaller particles (≈100 nm) at the surface of the SnO crystal could be the products of the reaction described in equation (4) and (5). However, no any other phases than SnO are observed on the XRD pattern, suggesting a minor oxidation of the material. So, the smaller particles probably come from the synthesis process. Due to their smaller size and more reactive surface, there are the ones which are susceptible to be more oxidized in surface, if any.
Micro SnO_2 powder is composed of round particles with a diameter between 50 and 200 nm. Nano SnO_2 power is very similar to the micro one but the particle diameter is in between 10 and 50 nm. An important particles size distribution is observed for all the commercial tin-based materials. Micro SnO_2 particles are on average 5 times bigger than nano SnO_2 particles which allow us to study the influence of particle size upon cycling.

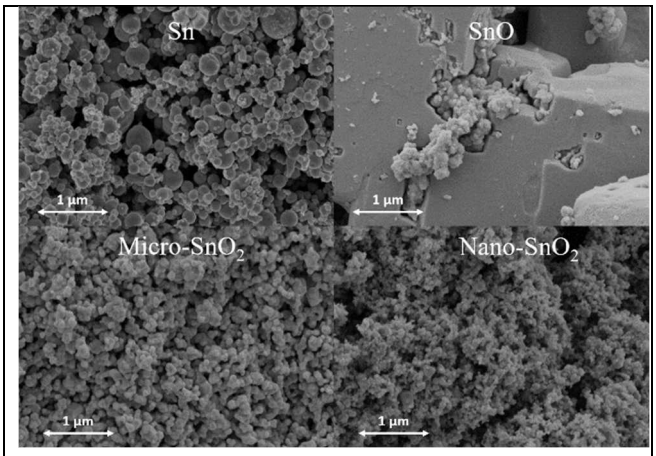

Fig. 2. SEM images of Sn, SnO, micro-SnO_2 and nano-SnO_2 at x10000 magnification.

3.2. Electrochemical properties

Galvanostatic electrochemical measurements were performed at 40 mA/g between 0.05 and 3V (vs Li/Li^+). Fig. 3 shows the first discharge and charge curves of Sn-based materials. The letters from (Fig. 3a) to (Fig. 3f) represent the different steps of the electrochemical mechanism of Li^+ with tin-based materials.

From (Fig. 3a) to (Fig. 3b), the conversion step occurs, then from (Fig. 3b) to (Fig. 3f) the alloying mechanism appears. The first cycle shows a great difference between the tin-based materials although a same alloying mechanism. Table 1 presents the number of moles of lithium exchanged during the first and the fifth discharges. To be able to compare the different tin-based materials, the conversion and the alloying processes have been separated for the calculation.

From (Fig. 3a) to (Fig. 3b), the first plateau (≈1V) observed in reduction can be attributed to the redox process of Sn (IV) or Sn (II) into Sn metal, the small plateau observed for Sn can be attributed to the reduction of surface oxide layer. Here we can clearly observe the amount of oxygen in tin-based materials with correlated Li_2O amount. The plateau length is proportional to the quantity of Li_2O formed during the conversion. Table 1 gives the number of Li^+ exchanged during the first discharge. The numbers of lithium exchanged are close to the expected one for all the tin-based materials. 1.9 Li^+ is obtained instead of a theoretical 2 for SnO, and respectively 3.46 and 3.03 for nano and micro-SnO_2, respectively, instead of 4. The number of lithium exchanged for Sn is 0.35 instead of 0 which could be due to the conversion of the small amount of SnO leading to a final composition for this material of $(SnO)_{0.175}Sn$.

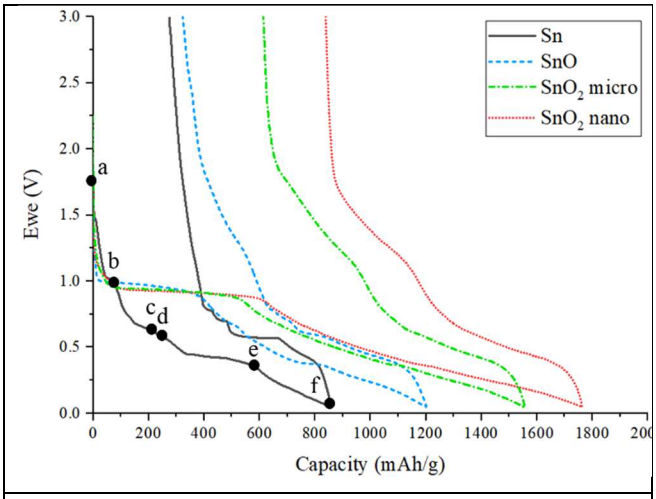

Fig. 3. First galvanostatic discharge/charge curves of Sn-based materials at 40 mA/g current density in the voltage range of 0.05-3V (vs Li/Li^+)

Table 1. Moles of lithium ion exchanged during the first and the fifth discharges for Sn, SnO, nano-SnO_2 and micro-SnO_2

Phases		E (V)	Theoretical $Li^+_{exchanged}$ for phase formation	Calculated $Li^+_{exchanged}$ during the discharge							
				Sn		SnO		Nano-SnO_2		Micro-SnO_2	
				1rst cycle	5th cycle	1rst cycle	5th cycle	1rst cycle	5th cycle	1rst cycle	5th cycle
Conversion	$SnO_x \rightarrow Sn$ + SEI (Fig. 3a)-(Fig. 3b)	OCV-0.9	2 (SnO) or 4 (SnO_2)	0.35	0	1.90	0	3.46	0	3.03	0
Alloying	Li-poor + SEI (Fig. 3b)-(Fig. 3e)	0.9-0.36	2.33	2.06	0.42	1.94	1.26	**2.80**	1.9	**2.52**	1.7
	Li-rich (Fig. 3e)-(Fig. 3f)	0.35-0.05	2.07	1.43	0.73	1.69	1.54	**2.28**	1.68	1.63	1.74
Total $nLi^+_{exchanged}$		3-0.05	4.4, 6.4 or 8.4 (1rst cycle) /4.4 (5th cycle)	3.84	1.15	5.53	2.8	**8.54**	3.58	7.18	3.44

The voltage where the Solid Electrolyte Interphase (SEI) is formed for tin-based material electrodes, is still discussed. Lucas et al. observed, with in situ Atomic Force Microscopy, AFM, on a tin electrode, the initial steps of the SEI formation from 2.5 V to 0.7 V (vs Li^+/Li) [13]. They also showed the instability of SEI layer on a Sn film. This phenomenon is enhanced by the large volume change upon cycling and gradual increase of the Specific Surface Area (SSA) [13]. Also with AFM, Beaulieu et al. found that the SEI can occur only before the formation of the first Li-Sn phase (Li_2Sn_5) (≈0.8V) which apparently has no catalytic surfaces that decompose electrolyte [18]. Ehinon et al. using both XPS and ^{119}Sn Mössbauer spectroscopy showed that the SEI consumed up to 4 moles of lithium at the very first stage of the discharge in case of Ni_3Sn_4 electrode [19]. The SEI formation in case of tin oxides cannot be dissociated from the conversion mechanism. Considering the works cited above, this study admits that the SEI occurs from the Open Circuit Voltage (OCV) to 0.7 V.

After the plateau from (Fig. 3b) to (Fig. 3f), under 0.9V, the general shape is similar for the different materials which suggests that a common mechanism exists. This part of the curve can be attributed to the Li-Sn alloying mechanism (2) [21]. The phase diagram of Li-Sn shows seven thermodynamically distinct phases ranging from lowest to highest lithium concentrations: Li_2Sn_5, LiSn, Li_7Sn_3, Li_5Sn_2, $Li_{13}Sn_5$, Li_7Sn_2 and $Li_{22}Sn_5$ [31]. According to the type of alloys formed, the specific capacity of the electrode could theoretically reach up to 994 mAh/g for $Li_{22}Sn_5$ [21]. However, the important volume change observed for the tin-based materials will increase with the highest lithium concentration in alloys. The volume change is not as severe when the Li-Sn phases are structurally related, for example in the case of the first two Li-Sn phases, Li_2Sn_5 (Fig. 3b)-(Fig. 3c) and LiSn (Fig. 3c)-(Fig. 3d) [8]. LiSn alloy is formed before 0.42V and a small plateau is observed testifying the formation of a stable phase [13]. This plateau can also be observed for SnO electrode but not for nano and micro SnO_2. The Li_2O insulating matrix slows down the conduction of electrons leading to a lesser separation of Li-Sn phase transitions. A larger plateau (Fig. 3d)-(Fig. 3e) is observed at 0.36 V corresponding to Li_7Sn_3 (Fig. 3d) phase formation. The alloys Li_2Sn_5, LiSn and Li_7Sn_3 are identified as lithium-poor phases. The lithium-rich phases (Fig. 3e)-(Fig. 3f), namely, Li_5Sn_2, $Li_{13}Sn_5$, Li_7Sn_2, and $Li_{22}Sn_5$, in the voltage range of 0.35 V to 0.05 V are structurally related and cannot be differentiated. Both Li-rich and Li-poor designation have been chosen according to Courtney et al. study [8]. Micro and nano-SnO_2 react with more than 8.4 theoretical lithium ion exchanged for the conversion and alloying mechanisms. The additional lithium ion amount can come either from the

reduction of the electrolyte to form the SEI or a new Li-rich phase at the lowest voltage due to nanostructuration. This last hypothesis should be studied in a further article.

The coulombic efficiencies of SnO and Sn are respectively 73% and 68% during the first cycle, whereas, the ones for nano and micro-SnO_2 are respectively 51% and 61% for the first cycle. The poor coulombic efficiency between the first discharge and charge is due to the irreversible conversion mechanism and also to SEI formation on Sn particles. The capacity loss during the first cycle is proportional to oxygen content in the respective materials which means that controlling the oxygen amount of the tin-base materials has a major impact on the first cycle which will induce the behavior of the material thereafter.

Polarization is less important in the case of SnO by comparison of SnO_2 materials because of the formation of less amount of Li_2O. Indeed, the electrically insulating nature of Li_2O which surrounds the Sn metallic clusters limit the Li^+ diffusion and the conductivity of the electrode [32]. Focusing on the SnO_2, the influence of the particles size can be observed. The first specific discharge of the nano-SnO_2 is more important than the micro-SnO_2 one. The plateau observed at 1V is longer for the nano-SnO_2 than in the case of micro-SnO_2, the conversion is more efficient. Moreover, the alloying + SEI part of the curve is also much longer for nano-SnO_2. However, the coulombic efficiency is smaller for nano-SnO_2 than for micro-SnO_2. Nanoparticles have a more important SSA which leads to the formation of a more important SEI and a smaller first cycle coulombic efficiency. Full conversion appears as not interesting for enhanced performances and limited Li_2O amount is required as in the case of SnO used as starting electrode material. The galvanostatic curves of the fifth cycle are shown in Fig SI1. The plateau lately observed around 1V has disappeared, testifying a high conversion of SnO_2 into Li_2O and Sn. However, the slopes at the early stages of the discharge are different which seem to show that the formation of the Li-poor alloys happens differently. Tin electrode has lost an important part of its discharge and charge capacity and the curve is very polarized. Micro-SnO_2 and nano-SnO_2 materials have a capacity of 777 mAh/g and 809 mAh/g, respectively, values quite close to the theoretical value of 994 mAh/g for tin alloying. In Table 1, the numbers of Li^+ exchanged after 5 cycles show that for Sn and SnO materials an important part of the lithium is not exchanged anymore. Aggregation in inactive particles seems to occur depending on the material composition. The capacity of the first reduction drives the performances of the next twenty cycles as shown in Fig. 4 except for SnO. Whatever the tin-based electrode, a bad coulombic efficiency and a small specific capacity are obtained after 100 cycles. Some clear improvement must be made if one wants to impose Sn-based materials in battery. The volume change leads to the loss of electronic contact between particles and current collector.

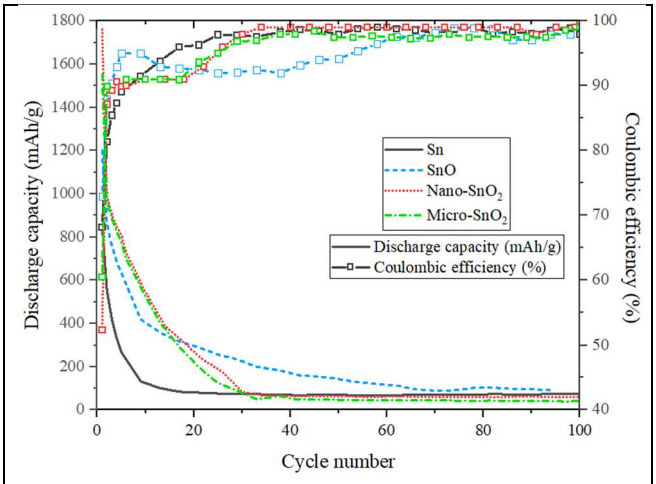

Fig. 4. Specific discharge capacity and coulombic efficiency as a function of cycle number at 40 mA/g current rate in the voltage range of 0.05-3V (vs Li/Li^+)

During cycling, the influence of Li_2O amount appears as critical. Specific capacity of SnO reaches and then exceeds specific capacity of SnO_2. After 20 cycles, specific capacities of Sn, SnO, nano-SnO_2 and micro SnO_2 are respectively 82 mAh/g, 287 mAh/g, 264 mAh/g and 215 mAh/g. The smaller quantity of Li_2O matrix in SnO allows the material to have a better cyclability, better coulombic efficiency and smaller polarization, indicating that Li_2O is needed but the amount should be limited. This can be done by controlling the oxidation state of the tin. An atomic O/Sn ratio close to 1 seems to be the best compromise. After 100 cycles, specific capacities of Sn, SnO, nano-SnO_2 and micro SnO_2 are respectively 74 mAh/g, 90 mAh/g, 60 mAh/g and 40 mAh/g. All tin-based materials have lost the major part of their specific capacity. Performances of nano-SnO_2 are about 50% more than micro-SnO_2 after 100 cycles, which seems to show some nanosizing benefit.

Galvanostatic tests at increasing current densities have been done in order to determine their power ability. Not to be limited by fading upon cycles, only one cycle at each increased C-rate has been conducted. A standard 3V voltage cell was used for power and energy density calculation. Such experiments allow the construction of a Ragone plot shown in Fig. 5, the results are summarized in Table 2. Raising current densities do not give charges enough time to migrate through pores which result in sluggish kinetics of electrochemical activities, so decreasing energy density must be obtained. Surprisingly, tin electrode doesn't withstand well the increasing C-rates since the lowest C-rates. Yet at C/10, tin electrode energy density is only of 200 Wh/kg. The energy density decrease is quite linear. However, the Sn electrode supports up to 3C current density and can recover 52% of its energy density when another cycle is made at C/25 after the

Table 2. Summay of the electrochemical properties of the different materials at different current densities.

Cycle number	Current density (mA/g)	Energy (Wh/kg)			
		Sn	SnO	Nano-SnO_2	Micro-SnO_2
1	40	615	1224	2001	1536
2	80	342	1086	1707	1248
3	160	207	1020	1284	921
4	320	126	927	945	495
5	640	72	759	564	21
6	1280	33	486	132	9
7	2560	15	135	21	3

last cycle at 3C. At small current densities from C/25 to C/5, tin oxide materials have the same energy density of about 1000 Wh/kg. At current densities higher than C/5, SnO electrode can support the different currents densities better

SnO_2 and micro SnO_2 are respectively 486 Wh/kg, 132 Wh/kg and 9 Wh/kg. It must be noticed that all the materials sustain 3C current density showing good ability to power applications and satisfying the VTOL specifications. Nanostructuration appears one more time as beneficial. The efficiency between the first cycle at 40 mA/g (C/25) and the last one after the current rate test is respectively for Sn, SnO, nano-SnO_2 and micro SnO_2 of 52%, 73%, 62% and 57%. SnO appears one more time as the most interesting electrode materials with rather good recovering properties.

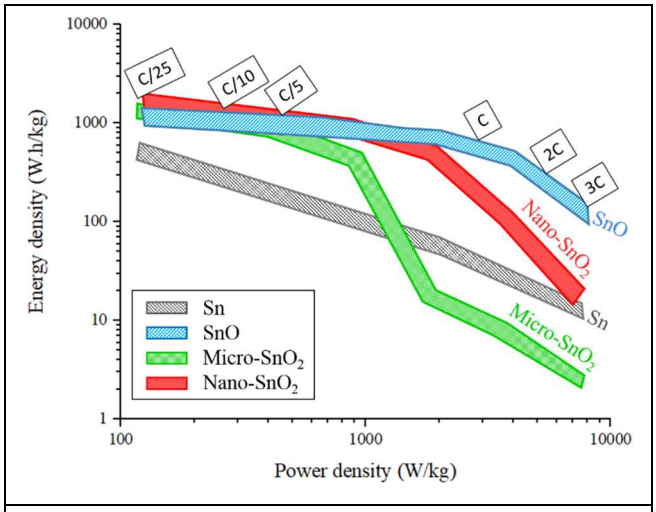

Fig. 5. Ragone plot of tin-based materials

The possible outcome of the tin-based materials is confirmed and especially under their oxide forms providing the stabilization of performances upon cycling.

3.3 Post mortem

The conversion mechanism and the quantity of Li_2O formed, linked to the oxygen amount in tin-based materials, seem to be the keys of these improved performances. After 100 cycles, the galvanostatic tests were stopped at the end of the oxidation process and the coin cells have been opened in order to evaluate the future failure mode. The electrodes have been washed using PC solvent and dried in argon atmosphere glovebox. To avoid air contamination, XRD measurements were performed in a special hermetic cell, so no contact with air or humidity happened before analysis. SEM analyses were performed under vacuum. The current collector is made of iron alloy and the corresponding peaks are indicated by a star on XRD patterns.

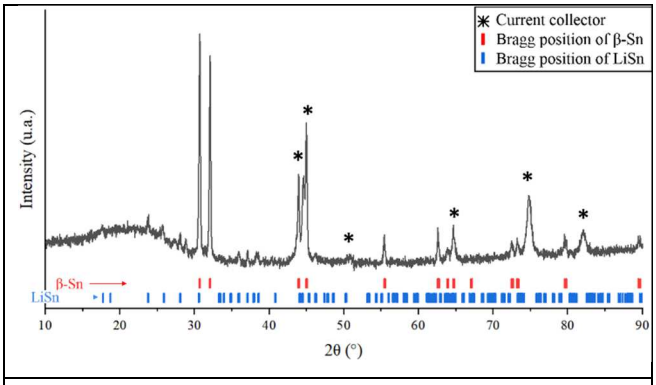

Fig. 6. XRD pattern of Sn electrode after 100 cycles.

Winter et al. demonstrated the degradation of tin electrodes upon cycling [10]. They observed with post-mortem microscopy characterizations the formation of cracks and electrode delamination. These cracks allowed the penetration of electrolyte between the current collector and the electrode material where it decomposed into insulating products. Because of the loss of electronic contact, lithium cannot be extracted anymore. In consequence, the amount of

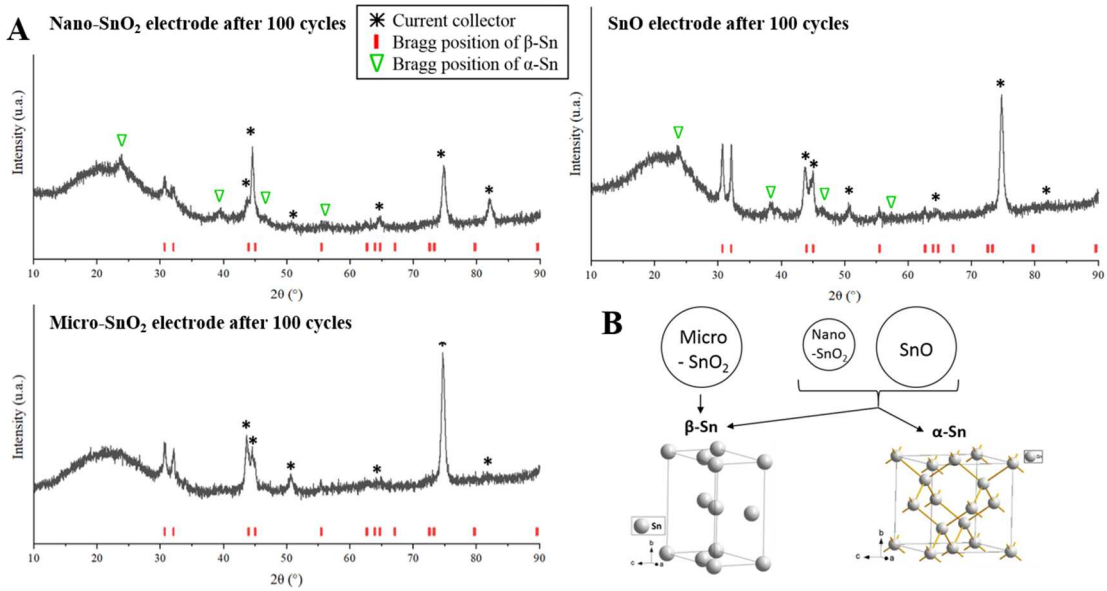

Fig. 7. (A) XRD patterns of SnO, nano-SnO_2 and micro-SnO_2 electrode before and after cycling. (B) Phases formation during conversion process for tin-oxide materials.

tin accessible for lithium storage decreases which explains the decreasing of the specific capacity upon cycling [21]. In case of tin oxide materials, in situ Transmission Electron Microscopy (TEM) managed by Huang et al. showed the important volume change upon lithiation on a single SnO_2 nanowire [33]. Furthermore, Courtney et al. showed that tin atoms aggregate into large coherent regions but these effects can be retarded in case of tin oxides [13] and nanostructured particles [20]. However, Retoux et al. using in situ AFM showed that the growth of tin clusters will lead to the loss of percolation paths and electronic contact in SnO_2 electrode during cycling [22].

These studies show the importance of in-situ and ex-situ characterizations in order to better understand the failure mode of Sn-based materials.

XRD patterns of the Sn electrode before cycling, as shown in Fig.1, can be fully indexed to β-Sn structure [26]. After cycling, the pattern presented in Fig.6 still correspond to the β-Sn structure, but another phase appears and can be indexed as LiSn monoclinic phase with P12/m1 space group (a_{th} = 5.17 Å, b_{th} = 3.18 Å, c_{th} = 7.74 Å) [13]. The LiSn phase formation has already been observed by Hu et al. in case of SnO_2 electrode [20]. As the electrode has been stopped at the end of the oxidation process, the presence of lithiated crystallized phase testifies the irreversibility of some alloying during cycling. This phenomenon testifies from the electrochemical grinding of the particles. The resulting loss of contact isolate the particles. The electrons cannot have accesses to the material anymore and the lithium cannot be extracted. XRD patterns of the SnO electrode before and after cycling, are also shown in Fig. 7. Before cycling SnO structure is observed. After cycling, the SnO structure is not visible anymore and new phases are observed. Conversion step has totally transformed the oxide form as it will be the case for all the oxide forms studied. The new phases form at the end of oxidation can be indexed as β-Sn, but also as cubic α-Sn with a space group of Fd-3m (a_{th} = 6.491 Å) [34]. XRD patterns of the nano-SnO_2 and micro-SnO_2 electrode before and after cycling are shown in Fig. 7. After cycling, nano-SnO_2 shows two phases similarly to SnO, whereas only β-Sn is registered for micro-SnO_2 in agreement with the literature [13]. The α-Sn formation isn't well known and has been much less reported. However, Oehl et al. showed for Sn/SnO_x nanoparticles that Sn nanoparticles can be transformed from the metallic β-structure to the semiconducting α-structure after lithium insertion and extraction. They discovered that the phase transition is size-related and is favored with decreasing particle size. They found that the critical size for this transformation is 17 nm [35]. In this study, the α-Sn is observed for nano-SnO_2 but not for micro-SnO_2 in agreement with the work of Oehl et al. The α-Sn structure is semiconducting, so the transformation will lead to an increase of the internal electric resistance of the electrode, which is unfavorable for electrochemistry. However, the nanosizing of particles has been proved as a good benefit for tin-based material cycling performances as shown in the first part of this study. More, Kaghazchi et al. showed that the more opened structure of α-Sn is kinetically more favorable for Li^+ insertion [34]. Legrain et al. confirmed this hypothesis with DFT calculations. [36]. The formation of the alpha phase seems therefore beneficial to electrochemical performance.

Up to now, α-Sn phase formation has not been reported for SnO material. The particles are mainly micrometric before cycling but both β-Sn and α-Sn are observed after cycling. We can already make two hypotheses. First, the partial surface oxidation of the unstable SnO particles allows the formation of nano-SnO_2 which can then be converted into α-Sn phase. Small particles of about 100 nm, probably oxidized on their surface, have been observed by SEM (Fig. 8) and can corroborate this hypothesis. Second, a very important particle division happen for SnO during the conversion step until nano-sizing which then can allow the formation of α-Sn phase. In both cases, SnO and nano-SnO_2, α-Sn phase formation seems to improve our performances compared to micro-SnO_2 or Sn electrode materials. This result is in line with the studies cited above.

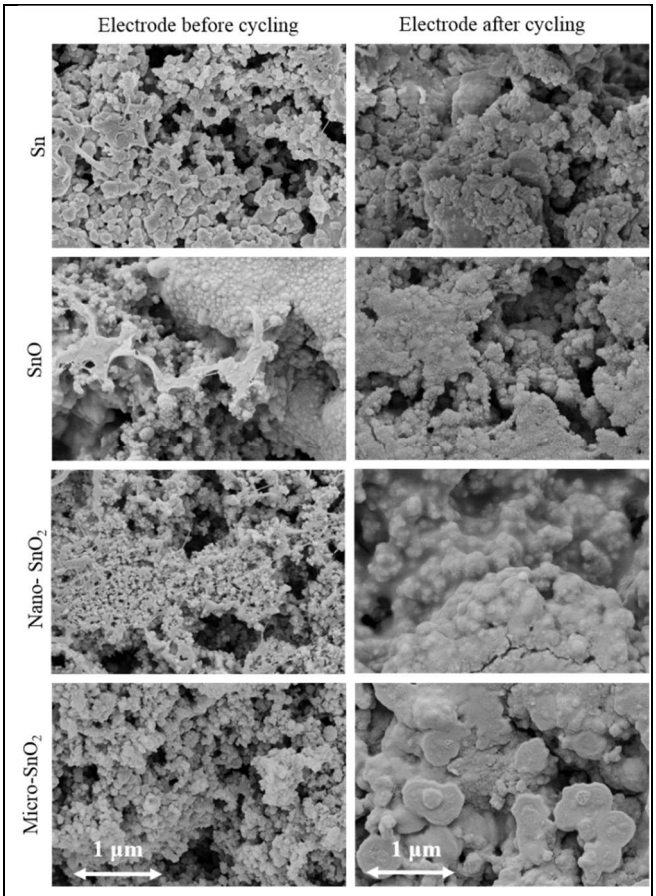

Fig. 8. SEM images of Sn, SnO, nano-SnO_2 and micro-SnO_2 electrodes before and after cycling

SEM images are shown in Fig. 8. Before cycling, spherical particles with an important distribution in size (50 nm to 500 nm) can be observed. Bridges between the particles are characteristic of PVDF binder. With SEM analysis, morphologies of Sn and carbon black are too close to identify their own contribution. To differentiate them, EDX images have been done. However, the magnification is smaller in this case because the surface of the beam interaction is bigger. EDX observations are shown in Fig. 9. For Sn electrode, red tin atoms are not homogeneously distributed in the blue carbon matrix. Oxygen atoms distribution is clearly linked with Sn one. After cycling, the raw morphology is lost. SEM images showed that the material seems to be aggregated in flake-like particles. Courtney et al. reported the aggregation of tin has a major drawback for tin electrode. Once large tin aggregates formed, the volume change upon cycling will be

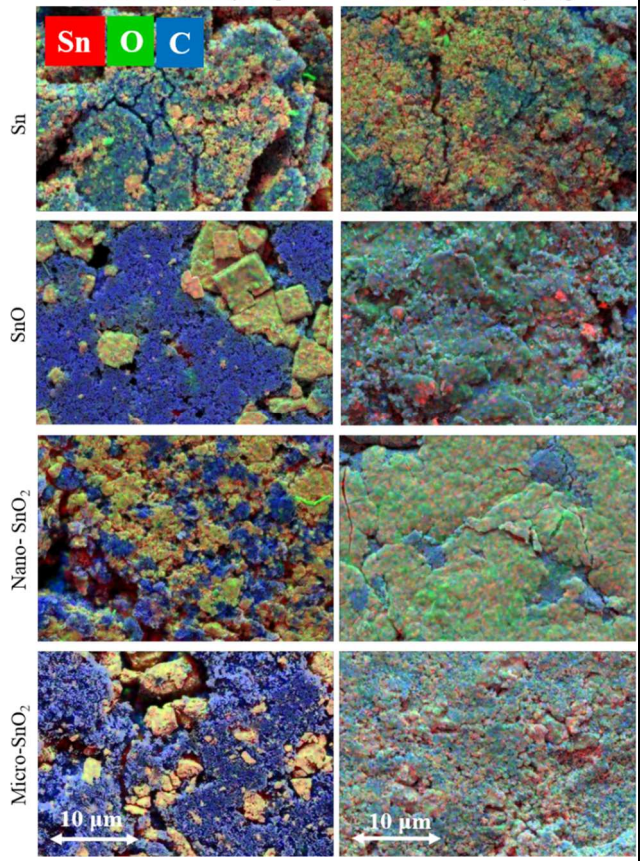

Fig. 9. EDX images of Sn, SnO, nano-SnO_2 and micro-SnO_2 electrodes before and after cycling

excessively increased which may induce cracking and capacity loss [13].

For SnO electrode before cycling, important particles corresponding to SnO can be observed (Fig. 8). All around these particles, really small ones identified as carbon black (<100nm) are connected with bridges (PVDF). EDX images are consistent with SEM images. The SnO particles can be easily distinguished from the carbon matrix. After cycling, the SEM pictures can testify the modifications already observed on XRD pattern. SnO particles have been crushed to form smaller particles. With EDX, the electrode after cycling shows a mixture of elements. The tin particles are included in a more amorphous matrix composed mainly of oxygen. Important red spots indicate the presence of tin aggregates. The important electrode amorphization undergone by SnO electrode could explain the α-Sn observation in the XRD pattern after cycling. In addition, it can explain the good cyclability of SnO electrode, small particles being known as interesting for electrochemistry [36]. SEM pictures of the nano-SnO_2 electrode before cycling show, as for SnO, spherical particles with a size <100 nm bound by wires identified as PVDF binder. EDX confirms this forecast. After cycling an important amorphization of the electrode is observed with SEM. Particles seem to have been aggregated and to be included into a matrix. The aggregates are bigger with a size higher than 100 nm. Images completed by EDX analysis have also been done and witness the elements mixing. SEM and EDX images of micro-SnO_2 before cycling showed that the electrode formulation is not homogeneous. After cycling, important aggregates are observed in SEM (>500nm). EDX show more red parts so more tin aggregates. SEM images are in agreement with XRD pattern, micro-SnO_2 even after the conversion its important particles size.

4. Conclusion

Electrochemical measurements have been made in the same conditions for different commercial tin-based materials. The results point out the very interesting performances in terms of energy and power density especially for the oxide forms of tin.

SnO appears as the best candidate concerning irreversible capacities and coulombic efficiency whereas SnO_2 has the best gravimetric capacity. A maximum of 2000 Wh/kg is obtained in terms of energy for nanostructured SnO_2 and if about 14 kWh is needed for VTOL, a battery weight of 7kg is imposed which is quiet reasonable. Low polarization is maintained in SnO whereas the high amount of insulating Li_2O, formed by the reduction of SnO_2, leads in increased polarization effect and decreased battery voltage.

Li_2O occurring seems essential to preserve Sn particles from aggregating and contributes to enhanced energy capability. However, the amount of oxygen atoms in oxide form must be controlled and an atomic O/Sn ratio close to 1 seems to be the most interesting case. Some complementary studies are needed to better evaluate this optimal ratio and to characterize Li_2O crystallinity, coverage, homogeneity by in situ HR-TEM coupled with electron diffraction.
Post-mortem characterizations demonstrate that complementary to O/Sn ratio, nanostructuration and α-Sn formation upon cycling are keys parameters for better performances.

Micro-SnO_2 and Sn appear as more sensitive to particles aggregations than nano-SnO_2 and SnO. Those latter two phases are able to be partially converted into α-Sn. To our knowledge, this phase has only been reported in case of nano-SnO_2 conversion. It is the first case that it has been reported starting from SnO.

Finally, if we go back to VTOLs applications requirements, the 3C maximal current density can be addressed for all the tin-based materials but the maintaining of an interesting capacity upon 1000 cycles is not sustainable for any tin-based oxide. Maybe, the current densities used were too high and those tests should be made at lower current densities. A better way of enhancement is to work on buffering by carbon matrix and to get compatible all the interphases by functionalization treatment such as fluorination in order to avoid aggregation upon cycling.

For vehicles applications, the study of tin-based materials over a wide temperature range should be performed. The effect of temperature for anode materials seems to focus on the reactivity of the interface. Temperature rise accelerates side reactions, reducing coulombic efficiency and cycle life. On the contrary, the SEI become less permeable to Li^+ at low temperatures, slowing down cell kinetics [38]. In case of Sn-based materials, Winter et al. reported excellent performances at high temperatures [14]. Jansen et al. observed the influence of lowered temperature on Sn-based intermetallic compared to graphite-based anode. All materials performances declined

drastically with decreasing temperature [39]. In addition, the cell polarization will be higher at low temperatures, increasing the energy inefficiency during cycling which is already problematic for tin-based materials. Recent reports on silicon materials suggests that silicon with high surface area and conductive coatings minimize some of these issues by reducing the lithium and electron diffusion path (despite the increase of SEI formation) [40], [41]. In consequence, nanostructuration and limitation of oxygen content can help tin-based materials to have a greater tolerance to low temperature.

ACKNOWLEDGMENTS

The authors acknowledge Joël Cellier, Rodolphe Thirouard and Malika El-Ghozzi for XRD measurements and interpretation and Suzanne Jacomet for the SEM and EDX observations. Thanks to Yajun Tao, Nicolas Demarthe and Benoit Cluzeau for supports in experiments.

REFERENCES

[1] D. Andre, H. Hain, P. Lamp, F. Maglia, and B. Stiaszny, 'Future high-energy density anode materials from an automotive application perspective', *J. Mater. Chem. A*, vol. 5, no. 33, pp. 17174–17198, Aug. 2017, doi: 10.1039/C7TA03108D.

[2] A. Mahmoudzadeh Andwari, A. Pesiridis, S. Rajoo, R. Martinez-Botas, and V. Esfahanian, 'A review of Battery Electric Vehicle technology and readiness levels', *Renew. Sustain. Energy Rev.*, vol. 78, no. C, pp. 414–430, 2017.

[3] 'Electric Flight – Potential and Limitations: AVT-209 Workshop, Lisbon, 22 – 24 October 2012 Dr. Martin Hepperle', *Scribd*.

[4] J. Thauvin, G. Barraud, X. Roboam, B. Sareni, M. Budinger, and D. Leray, 'Hybrid propulsion for regional aircraft: A comparative analysis based on energy efficiency', in *2016 International Conference on Electrical Systems for Aircraft, Railway, Ship Propulsion and Road Vehicles International Transportation Electrification Conference (ESARS-ITEC)*, Nov. 2016, pp. 1–6, doi: 10.1109/ESARS-ITEC.2016.7841392.

[5] U. Elevate, 'Fast-forwarding to a future of on-demand urban air transportation', *Uber Com*, 2016.

[6] A. Bacchini and E. Cestino, 'Electric VTOL Configurations Comparison', *Aerospace*, vol. 6, no. 3, p. 26, Mar. 2019, doi: 10.3390/aerospace6030026.

[7] 'EHang | UAM - Passenger Autonomous Aerial Vehicle (AAV)'. https://www.ehang.com/ehangaav/ (accessed Jun. 09, 2020).

[8] G. E. Blomgren, 'The Development and Future of Lithium Ion Batteries', *J. Electrochem. Soc.*, vol. 164, no. 1, p. A5019, Dec. 2016, doi: 10.1149/2.0251701jes.

[9] T. Placke, R. Kloepsch, S. Dühnen, and M. Winter, 'Lithium ion, lithium metal, and alternative rechargeable battery technologies: the odyssey for high energy density', *J. Solid State Electrochem.*, vol. 21, no. 7, pp. 1939–1964, Jul. 2017, doi: 10.1007/s10008-017-3610-7.

[10] J. M. Tarascon, 'The Li-Ion Battery: 25 Years of Exciting and Enriching Experiences', *Electrochem. Soc. Interface*, vol. 25, no. 3, p. 79, Jan. 2016, doi: 10.1149/2.F08163if.

[11] T. Kim, W. Song, D.-Y. Son, L. K. Ono, and Y. Qi, 'Lithium-ion batteries: outlook on present, future, and hybridized technologies', *J. Mater. Chem. A*, vol. 7, no. 7, pp. 2942–2964, Feb. 2019, doi: 10.1039/C8TA10513H.

[12] B. Huang, Z. Pan, X. Su, and L. An, 'Tin-based materials as versatile anodes for alkali (earth)-ion batteries', *J. Power Sources*, vol. 395, pp. 41–59, Aug. 2018, doi: 10.1016/j.jpowsour.2018.05.063.

[13] I. A. Courtney and J. R. Dahn, 'Electrochemical and In Situ X-Ray Diffraction Studies of the Reaction of Lithium with Tin Oxide Composites', *J. Electrochem. Soc.*, vol. 144, no. 6, pp. 2045–2052, Jan. 1997, doi: 10.1149/1.1837740.

[14] M. Winter and J. Besenhard, 'Electrochemical lithiation of tin and tin-based intermetallics and composites', *Electrochimica Acta*, vol. 45, no. 1–2, pp. 31–50, 1999, doi: 10.1016/S0013-4686(99)00191-7.

[15] I. A. Courtney and J. R. Dahn, 'Key Factors Controlling the Reversibility of the Reaction of Lithium with SnO2 and Sn2 BPO 6 Glass', *J. Electrochem. Soc.*, vol. 144, no. 9, pp. 2943–2948, Jan. 1997, doi: 10.1149/1.1837941.

[16] I. A. Courtney, W. R. McKinnon, and J. R. Dahn, 'On the Aggregation of Tin in SnO Composite Glasses Caused by the Reversible Reaction with Lithium', *J. Electrochem. Soc.*, vol. 146, no. 1, p. 59, Jan. 1999, doi: 10.1149/1.1391565.

[17] Y. Idota, T. Kubota, A. Matsufuji, Y. Maekawa, and T. Miyasaka, 'Tin-Based Amorphous Oxide: A High-Capacity Lithium-Ion-Storage Material', *Science*, vol. 276, no. 5317, pp. 1395–1397, May 1997, doi: 10.1126/science.276.5317.1395.

[18] P. Poizot, S. Laruelle, S. Grugeon, L. Dupont, and J.-M. Tarascon, 'Nano-sized transition-metal oxides as negative-electrode materials for lithium-ion batteries', *Nature*, vol. 407, no. 6803, pp. 496–499, Sep. 2000, doi: 10.1038/35035045.

[19] H. Kim *et al.*, 'Comparative study of bulk and nano-structured mesoporous SnO2 electrodes on the electrochemical performances for next generation Li rechargeable batteries', *J. Power Sources*, vol. 413, pp. 241–249, Feb. 2019, doi: 10.1016/j.jpowsour.2018.12.035.

[20] R. Hu *et al.*, 'Dramatically enhanced reversibility of Li2O in SnO2-based electrodes: the effect of nanostructure on high initial reversible capacity', *Energy Environ. Sci.*, vol. 9, no. 2, pp. 595–603, Feb. 2016, doi: 10.1039/C5EE03367E.

[21] M. Winter and J. Besenhard, 'Electrochemical lithiation of tin and tin-based intermetallics and composites', *Electrochimica Acta*, vol. 45, no. 1–2, pp. 31–50, 1999, doi: 10.1016/S0013-4686(99)00191-7.

[22] R. Retoux, T. Brousse, and D. M. Schleich, 'High-resolution electron microscopy investigation of capacity fade in SnO2 electrodes for lithium-ion

batteries', *J. Electrochem. Soc.*, vol. 146, no. 7, pp. 2472–2476, Jul. 1999, doi: 10.1149/1.1391957.

[23] D.-S. Wu, C.-Y. Han, S.-Y. Wang, N.-L. Wu, and I. A. Rusakova, 'Microwave-assisted solution synthesis of SnO nanocrystallites', *Mater. Lett.*, vol. 53, no. 3, pp. 155–159, Mar. 2002, doi: 10.1016/S0167-577X(01)00468-2.

[24] M. Zhang, T. Wang, and G. Cao, 'Promises and challenges of tin-based compounds as anode materials for lithium-ion batteries', *Int. Mater. Rev.*, vol. 60, no. 6, pp. 330–352, Aug. 2015, doi: 10.1179/1743280415Y.0000000004.

[25] L. Liu, F. Xie, J. Lyu, T. Zhao, T. Li, and B. G. Choi, 'Tin-based anode materials with well-designed architectures for next-generation lithium-ion batteries', *J. Power Sources*, vol. 321, no. Supplement C, pp. 11–35, Jul. 2016, doi: 10.1016/j.jpowsour.2016.04.105.

[26] J. A. Lee and G. V. Raynor, 'The Lattice Spacings of Binary Tin-Rich Alloys', *Proc. Phys. Soc. Sect. B*, vol. 67, no. 10, pp. 737–747, Oct. 1954, doi: 10.1088/0370-1301/67/10/301.

[27] G. Schmuelling *et al.*, 'Synthesis and electrochemical performance of surface-modified nano-sized core/shell tin particles for lithium ion batteries', *Nanotechnology*, vol. 25, no. 35, p. 355401, Sep. 2014, doi: 10.1088/0957-4484/25/35/355401.

[28] W. E. Boggs, P. S. Trozzo, and G. E. Pellissier, 'The Oxidation of Tin', *J. Electrochem. Soc.*, vol. 108, no. 1, p. 13, 1961, doi: 10.1149/1.2428003.

[29] C. M. Campo, J. E. Rodríguez, and A. E. Ramírez, 'Thermal behaviour of romarchite phase SnO in different atmospheres: a hypothesis about the phase transformation', *Heliyon*, vol. 2, no. 5, p. e00112, May 2016, doi: 10.1016/j.heliyon.2016.e00112.

[30] M. S. Moreno, G. Punte, G. Rigotti, R. C. Mercader, A. D. Weisz, and M. A. Blesa, 'Kinetic study of the disproportionation of tin monoxide', *Solid State Ion.*, vol. 144, no. 1, pp. 81–86, Sep. 2001, doi: 10.1016/S0167-2738(01)00882-7.

[31] J. Sangster and C. W. Bale, 'The Li-Sn (Lithium-Tin) system', *J. Phase Equilibria*, vol. 19, no. 1, p. 70, Feb. 1998, doi: 10.1361/105497198770342788.

[32] C. J. Pelliccione, E. V. Timofeeva, and C. U. Segre, 'Potential-Resolved In Situ X-ray Absorption Spectroscopy Study of Sn and SnO2 Nanomaterial Anodes for Lithium-Ion Batteries', *J. Phys. Chem. C*, vol. 120, no. 10, pp. 5331–5339, Mar. 2016, doi: 10.1021/acs.jpcc.5b12279.

[33] J. Y. Huang *et al.*, 'In situ observation of the electrochemical lithiation of a single SnO_2 nanowire electrode', *Science*, vol. 330, no. 6010, pp. 1515–1520, Dec. 2010, doi: 10.1126/science.1195628.

[34] S. Sabet and P. Kaghazchi, 'Communication: Nanosize-induced restructuring of Sn nanoparticles', *J. Chem. Phys.*, vol. 140, no. 19, p. 191102, May 2014, doi: 10.1063/1.4878735.

[35] N. Oehl, L. Hardenberg, M. Knipper, J. Kolny-Olesiak, J. Parisi, and T. Plaggenborg, 'Critical size for the β- to α-transformation in tin nanoparticles after lithium insertion and extraction', *CrystEngComm*, vol. 17, no. 19, pp. 3695–3700, 2015, doi: 10.1039/C5CE00148J.

[36] Q. Zhao, L. Ma, Q. Zhang, C. Wang, and X. J. Xu, 'SnO2 -Based Nanomaterials: Synthesis and Application in Lithium-Ion Batteries and Supercapacitors', *J. Nanomater.*, vol. 2015, pp. 1–15, May 2015, doi: 10.1155/2015/850147.